Poster 5690

Characterization of Tumor Growth and Immune Microenvironment in Humanized NOG-EXL Mice Implanted with A549, MDA-MB-436, and A375 Cells

Srimoyee Ghosh[1], Ann Fiore[2], Christoph Eberle[2], Sarah Wang[1], Keith Mikule[1], Kristen McEachern[1], Sujatha Kumar[1], David Jenkins[1]*, Geeta Sharma[2]*

[1]TESARO, Inc., Waltham, MA; [2]Charles River Laboratories, Worcester, MA

*Cosenior author

Introduction

Syngeneic mouse models have been the mainstay for immuno-oncology (IO) research. These models can be established relatively easily in immunocompetent hosts to evaluate the mechanism of action and efficacy of IO treatments. Although utilized extensively for preclinical evaluation, these models have several limitations: 1) these are murine tumors with murine targets; 2) most of the tumor cell lines grow rapidly in vivo, thus limiting studies to short dosing durations before tumor volumes reach Institutional Animal Care and Use Committee–defined limits, both of which do not mimic human tumors; 3) very few cancer types and cell lines are available for testing limiting the diversity of evaluable cancers, and only a few have been found to be responsive to current IO treatments (eg, MC38, CT26, and EMT-6); and 4) only the murine surrogate of the human antibody/protein can be evaluated.[1,2]

Subsequent to the development of severely immunodeficient mouse strains harboring mutations in the interleukin (IL)-2 receptor common γ gene locus, humanized mice have emerged as an alternative model. It is possible to engraft these mice with human hematopoietic stem cells (HSCs) that develop into functional human immune systems. There are 3 approaches for engrafting human immune systems into immunodeficient IL2rg^{null} mice: injection of peripheral blood leukocytes; injection of CD34$^+$ human stem cells derived from umbilical cord blood; and the bone marrow/liver/ thymus ("BLT") model, established by transplanting human fetal liver and thymus under the kidney capsule and intravenously injecting autologous fetal liver HSCs. An important addition to the immunodeficient IL2rg^{null} mice was to add the ability to express human granulocyte-macrophage colony-stimulating factor (hGM-CSF) and human IL-3 cytokines to support myeloid lineage engraftment after HSC implantation.[3]

In this study, we utilized hGM-CSF/IL-3 NOG mice (Taconic, NY) engrafted with human CD34$^+$ HSCs, which have been shown to stably develop human cell lineages 12 weeks after implantation. These mice are shipped when the human CD45$^+$ (hCD45$^+$) is observed to be ≥25% in peripheral blood. These humanized mice offer the opportunity to study tumor immune system interactions in vivo in mice with engrafted tumor cells and established human immune systems, thus enabling the interrogation of tumor interaction with the immune system, mechanism of tumor escape, and therapeutic potential of immune modulation,[3] all of which are critical for the development of IO drugs.

Here, we evaluated tumor growth in huNOG-EXL mice implanted with 3 different cell lines: A549 (human epithelial lung carcinoma), MDA-MB-436 (triple-negative human mammary adenocarcinoma), and A375 (human melanoma). To understand the tumor microenvironment in these mice, we profiled the tumors for lymphoid and myeloid cells using flow cytometry. The splenic compartment was also immune profiled to evaluate the correlation, if any, between the tumor and the peripheral immune compartments. Finally, based on the tumor infiltrate, we evaluated the CDX models for immunologic activity.

Methods

Twelve-week-old huNOG-EXL (NOD.Cg-*Prkdcscid Il2rgtm1Sug* Tg(SV40/HTLV-IL3, CSF2)10-7Jic/JicTac) mice having ≥25% hCD45$^+$ in peripheral blood mice were procured from Taconic, NY. The mice were inoculated with A549, MDA-MB-436, and A375 cells subcutaneously in the flank region at a cell density of 5x10^6 cells per mouse with Matrigel (Cat.354234; Corning). The tumors were measured using vernier calipers, and the tumor volume was calculated with the formula 1/2(length × width^2).

The animals were euthanized using institutional guidelines, and the tumors were collected at a tumor volume of 1000 mm^3–1500mm^3. Spleens and tumor tissue were collected and processed for flow cytometry.

For flow cytometry, spleens and tumors were dissociated into single-cell suspensions using gentleMACS (Miltenyi Biotech, MA). Cells were stained with a cocktail of antihuman antibody conjugates for surface marker staining. For intracellular staining, the cells were fixed and permeabilized using the Foxp3 staining buffer set (ThermoFisher, MA). For intracellular cytokine staining, cells were stimulated with the Cell Stimulation and Protein Transport Inhibitor Cocktail (ThermoFisher, MA) and stained for cytokines after appropriate fixation and permeabilization. Single cell and fluorescence minus one controls were processed in parallel. Following instrument setup and compensation, samples were acquired using the Attune NxT Flow Cytometer 4-laser system (ThermoFisher, MA). Post-acquisition analyses were performed using FlowJo v10.4 (FlowJo) for gating and GraphPad Prism (GraphPad Software) for data representation.

Results

The composition of immune cell types greatly varied in spleen and the tumor microenvironment between the three humanized models analyzed. Stronger cytokine responses to PMA/Ionomycin stimulation were observed in spleen and tumor samples obtained from the A375 model. Overall, for assessing myeloid and lymphoid phenotypes in spleen the A549 model provided the most consistent results. On the other hand, the A375 model was found as the one with the highest number of CD45$^+$ cells, when phenotyping both the myeloid and lymphoid compartment of tumor infiltrates. Highest CD8$^+$ T-cell frequencies were found in spleen and tumors collected from MDA-MB-436–inoculated mice.

Figure 1. Tumor Growth Curves Demonstrating Successful Engraftment and Tumor Growth in huNOG-EXL Mice Implanted with (A) A549, (B) MDA-MB-436, and (C) A375 Cells.

Tumor measurement was initiated at a tumor volume of 80 mm^3–100 mm^3 after which the tumors were measured twice weekly. Mice were euthanized at a tumor volume of 1000 mm^3-1500 mm^3 to collect tumors and spleens for immunophenotyping.

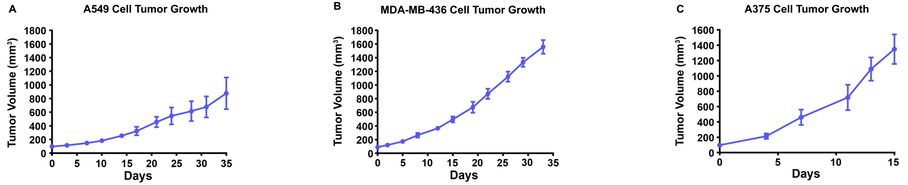

Figure 2. Lymphoid and Myeloid Cells and Intracellular Cytokine–Expressing Cells were Identified in Spleens and Tumors from Tumor Cell Line-Inoculated Mice.

Column A: Lymphoid, myeloid, and intracellular cytokine-expressing cell populations as a percentage of total CD45$^+$ cells from tumors and spleens in A549 cell inoculated mice. Column B: Lymphoid and myeloid cell populations as a percentage of total CD45$^+$ cells from tumors and spleens in MDA-MB-436 cell inoculated mice (Samples from these mice were not processed for intracellular cytokine signaling). Column C: Lymphoid, myeloid, and intracellular cytokine-expressing cell populations as a percentage of total CD45$^+$ cells from tumors and spleens in A375 cell inoculated mice.

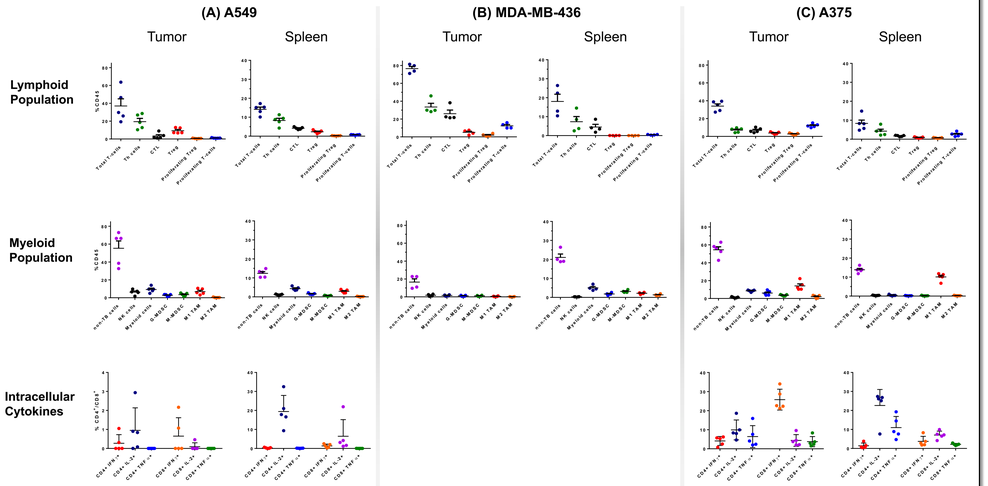

Figure 3. Gating Strategy for Lymphoid Cell Subsets from Splenocytes Obtained from huNOG-EXL Mice.

(**A**) Doublets using FSC-A and FSC-H plots (**B**) and dead cells using a fixable viability dye (**C**) were excluded from the splenocyte analysis. Starting from CD45$^+$ lymphocytes (**D**) total T-cells were gated as CD3$^+$ cells (**E**). The latter population was divided by CD4 and CD8 expression (**F**), defining 2 major subsets: helper T-cells (Th cells; CD4$^+$CD8$^-$) and cytotoxic T-cells (CTL; CD8$^+$CD4$^-$). CD4$^+$FoxP3$^+$ events were defined as Treg cells (**G**). Gating for Ki67 gave proliferating Treg (**H**) and proliferating total T-cells (**I**).

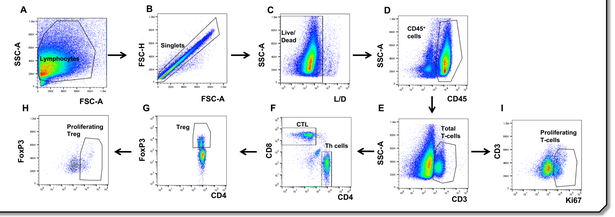

Figure 4. Gating Strategy for Myeloid Cell Subsets from Splenocytes Obtained from huNOG-EXL Mice.

(**A**) Doublets using FSC-A and FSC-H plots (**B**) and dead cells using a fixable viability dye (**C**) were removed from the splenocyte analysis. CD45$^+$ cells were first gated (**D**) and subsequently split into CD3$^+$CD20$^+$ and CD3$^-$CD20$^-$ populations (**E**). Out of the CD3$^-$CD20$^-$ population, NK cells were identified by CD56 expression (**F**). HLA-DR events were divided by CD14 (**G**) expression and then defined as G-MDSC and M-MDSC based on their CD33 phenotype (**I**). From an CD14$^-$ HLA-DR$^+$ subset (**H**), M1 and M2 macrophages were gated as CD68$^+$CD206$^-$ cells (**J**) and CD68$^+$HLA-DR$^+$ cells (**K**).

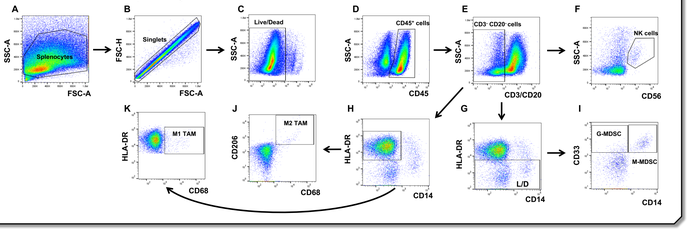

Figure 5. Gating Strategy for Cytokine-Expressing T-cell Subsets from Splenocytes Obtained from huNOG-EXL Mice.

Initially, (**A**) doublets using FSC-A and FSC-H plots (**B**) and dead cells using a fixable viability dye (**C**) were removed from the splenocyte analysis. Total T-cells were first gated as CD3$^+$ population (**D**), which were split by CD4 and CD8 expression (**E**). Subsequently, the proportion of IFN-γ, TNF-α, and IL-2 secretion, respectively, were evaluated to identify CD4$^+$ T-cells (**F-G**) and CD8$^+$ T-cells (**H-I**) producing IFN-γ, IL-2, or TNF-α.

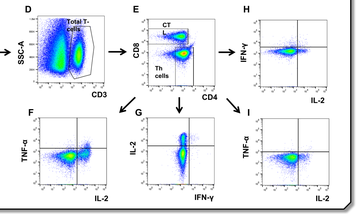

Conclusions

- huNOG-EXL mice supported the tumor engraftment and growth of 3 different human cell lines, A549, MDA-MB-436, and A375.
- Lymphoid cell subsets CD4, CD8, regulatory T-cells, and proliferating cells could be identified in both the splenic and tumor compartments of the huNOG-EXL mice implanted with various tumor cell lines.
- Limited myeloid cell populations were observed in both the spleens and the tumors. The percentage of M1 macrophages was found to be more than myeloid-derived suppressor cells (both G and M) and M2 macrophages.
- Cytokine (interferon-g, IL-2, and tumor necrosis factor-a)-secreting CD8$^+$ cells were seen in splenocytes activated with phorbol myristate acetate-ionomycin in A549 and A375 models.
- The results demonstrated that huNOG-EXL mice could be useful tools to dissect the immune response in human tumors. It was possible to identify and quantitate the myeloid cells that are absent in models implanted with human peripheral blood mononuclear cells instead of human CD34 stem cells.

References

1. Li QX, et al. *Pharmacol Ther.* 2017;173:34-46.
2. Sanmamed MF, et al. *Ann Oncol.* 2016;27:1190-8.
3. Walsh NC, et al. *Annu Rev Pathol.* 2017;12:187-215.

Acknowledgments

This study was sponsored and funded by TESARO, Inc. Formatting and editorial support, funded by TESARO, Inc., were provided by Ashfield Healthcare Communications, Middletown, CT, USA.